On The Influence of Laser-Drive Parameters on Annular Fast Electron Transport in Solids

Contact: paul.mckenna@strath.ac.uk

D. A. MacLellan, D. C. Carroll, R. J. Gray and P. McKenna
Department of Physics,
SUPA,
University of Strathclyde,
Glasgow G4 0NG, UK

A. P. L. Robinson and D. Neely
Central Laser Facility,
STFC Rutherford Appleton Laboratory,
Oxfordshire OX11 0QX, UK

M. P. Desjarlais
Sandia National Laboratories,
P.O. Box 5800,
Albuquerque, New Mexico,
87185, USA

Abstract

Annular fast electron transport in silicon is investigated as a function of the laser-drive pulse parameters using three-dimensional hybrid particle-in-cell (PIC) simulations. By varying the laser energy, focal spot radius and pulse duration we report that annular transport is accutely sensitive to the peak laser intensity, emphasising the key relationship between fast electron transport properties and the laser-drive parameters explored. These results may have implications for fast ignition and ion-acceleration schemes.

Introduction

The propagation of relativistic (i.e. fast) electrons, driven by an ultraintense laser pulse, through a solid gives rise to the formation and evolution of strong electromagnetic fields, often at large distances (e.g. 100 μm) from the interaction region (i.e. fast electron source). The transport properties of these electrons are therefore important for applications, such as the fast ignition approach to inertial confinement fusion [1] and the properties of beams of sheath-accelerated ions [2].

Recently, we demonstrated that the resistivity of the solid at relatively low temperatures ($\sim$ few eV) can predominantly define the fast electron transport properties [3, 4, 5].

In this report we numerically investigate, using 3D hybrid particle-in-cell (PIC) simulations, the sensitivity of annular fast electron beam transport to the parameters of the drive laser pulse. We observe and quantify variations to the size (i.e. radius) of the ring and the density of the electrons forming it as a function of laser pulse energy, duration and focal spot radius. The resulting trends are understood within the framework of the effects of resistively generated magnetic fields.

Modelling

The simulations are performed using the ZEPHYROS code [6]. For each simulation case, the fast electrons propagate in the X-direction with an exponential energy distribution (of the form $\exp(-\frac{E}{T_f})$, where E is the electron kinetic energy) and the mean temperature T_f scales ponderomotively [7]. The electrons are injected with a uniform angular distribution over a cone subtended by a half-angle of 50° [8] and in all cases the initial target temperature is set equal to 1 eV.

The silicon resistivity-temperature profile used in the simulations, shown in figure 1(a), is obtained from quantum molecular dynamics (QMD) simulations and subsequent wide range Kubo-Greenwood resitivity calculations [9], as discussed in MacLellan *et al.* [4]. In that work, it was shown that the dip in resistivity at temperatures as low as a few eV leads to a reversal in the resistivity gradient near the edges of the fast electron beam (where the target is heated to relatively low temperatures).

Example hybrid-PIC simulation results showing 2D maps (for $I_L = 5 \times 10^{20}$ Wcm^{-2}; $E_L = 192$ J; $\tau_L = 1$ ps and $r_L = 3.5$ μm) are displayed in figure 1, corresponding to: (b, c) $\log_{10}$ fast electron density (m^{-3}), in the [X-Y] mid-plane and [Y-Z] rear surface plane respectively; (d) temperature profile (in eV); and (e) corresponding map of magnetic flux density (in Tesla). The reversal of the resistivity gradient generates a reversal in the direction of the resistive magnetic field. The combination of the collimating effect of the azimuthal magnetic field enveloping the beam and the reversed magnetic field just inside the edge of the beam, drive a localized increase in the fast electron beam current density in an annular profile [4]. When the annulus contains a significant fraction of the total electron current, the transport pattern is maintained and even reinforced as the electrons propagate through the target. This reinforcement occurs

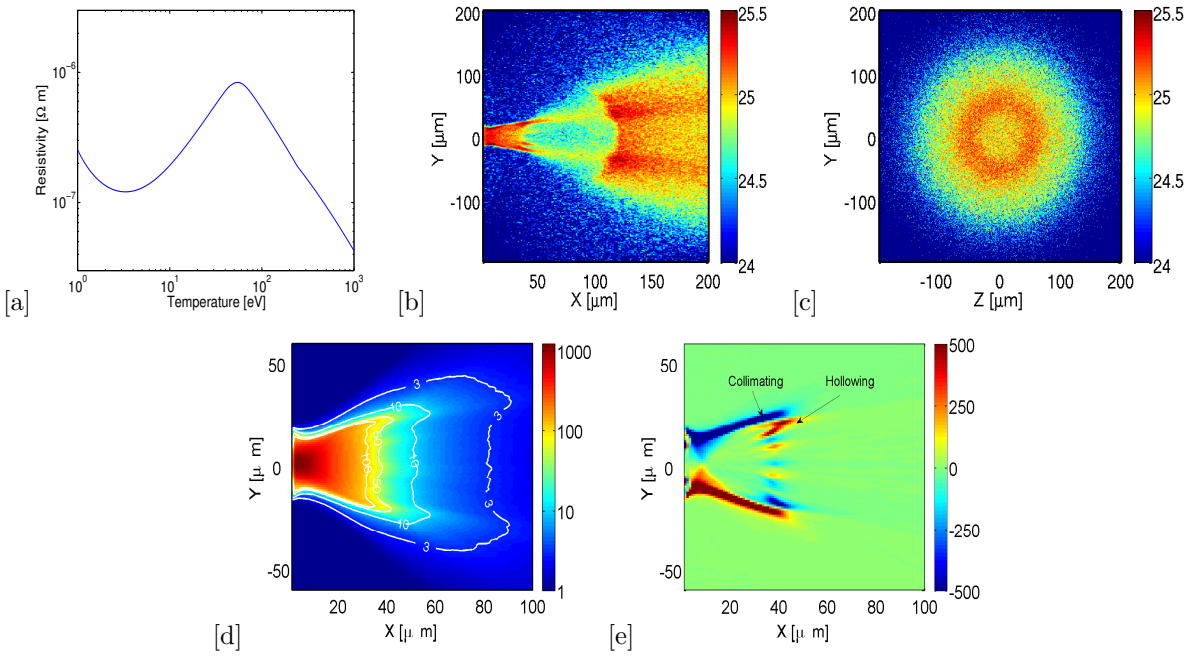

Figure 1: (a) Electrical resistivity of silicon as a function of temperature, calculated utilising *ab initio* QMD calculations [4]. Example hybrid-PIC simulation results showing 2D maps (at 1400 fs) of: (b, c) $\log_{10}$ fast electron density (m^{-3}) in the [X-Y] mid-plane and [Y-Z] rear surface plane; (d) target temperature (in eV), with selected isothermal contours; and (e) the corresponding magnetic flux density (B_Z component in Tesla), displaying two components: 1) a collimating component which acts to limit the divergence of the beam; and 2) a hollowing component arising from a reversal in the magnetic field direction inside the edge of the beam.

due to the localised increase in resistive heating arising from the increase in $\mathbf{j}_f$ (since resistive heating scales as $\mathbf{j}_f^2$), and thus larger resistivity gradients and azimuthal B-fields surrounding the annulus.

Simulation Results

To quantify the annular transport present in the simulation results, two parameters are defined: (1) the inner radius of the annulus; and (2) the ratio of the electron densities in the annulus to the axial position ([200,0,0]), both evaluated at the end of the simulation box (i.e. at X = 200 μm). Together, these quantities effectively quantify the size of the ring and the annulus-to-axial electron density contrast ratio.

The sensitivity of these parameters to the drive laser pulse parameters is explored by performing three simulation scans: A) variation of laser pulse energy, E_L in the range 78 - 385 J, for fixed focal spot radius $r_L = 3.5$ μm and fixed laser pulse duration $\tau_L = 1$ ps; B) variation of r_L in the range 2.5 - 5.5 μm, for fixed $E_L = 192$ J and $\tau_L = 1$ ps; and, C) variation of τ_L in the range 0.5 - 2.5 ps, for fixed $E_L = 192$ J and $r_L = 3.5$ μm. These parameter ranges were selected such that the peak laser pulse intensity, I_L, was varied in the range 2×10^{20} - 1×10^{21} Wcm^{-2} for all three scans. To examine these trends in greater detail, the rear-surface fast electron density simulation outputs are analysed to quantify the variation of the size of the annulus and the relative density of electrons contained within it, as a function of I_L for each of the three scans the results are shown in figure 2(a). Figure 2(b) shows the ratio of the fast electron density in the annulus (peak density) to the density of the centre of the beam, [Y, Z] = [0, 0].

For variation of laser-drive energy (i.e. scan A), increasing the energy from 78 J to 385 J produces an overall increase in the divergence of the electron beam and thus an increase in the radius of the annulus. By contrast, for increasing the intensity over the same range (by decreasing the focal spot radius from $r_L = 5.54$ μm to 2.48 μm (i.e. scan B)) the increase in both the overall beam divergence and the radius of the ring is smaller – the fixed laser pulse energy in combination with the increasing laser intensity results in fewer electrons injected for decreasing focal spot radius. As a consequence the target temperature and resistivity evolution, and thus subsequent electron transport properties, changes. In scan C, significant changes in the beam transport are found for variation of the pulse duration. As τ_L is increased, the overall beam divergence and radius of the annular structure decrease, leading to a more uniform beam transport for increasing pulse duration.

The overall increase in the ring radius with increasing peak laser intensity, present for all three scans, is due to

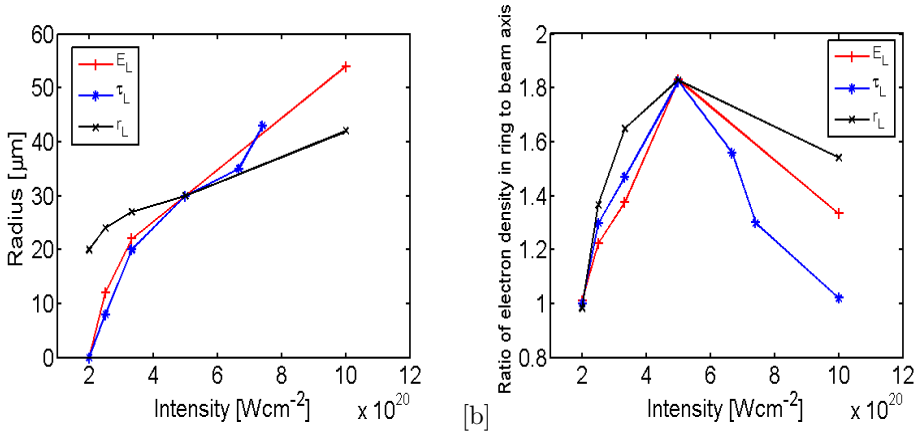

Figure 2: (a) Inner radius of the annulus at the target rear surface as a function of I_L, for the three parameter scans. (b) Ratio of the fast electron density in the annulus to the density on-axis (i.e. at [200,0,0]) as a function of I_L, for the same three parameter scans.

the increase in the divergence of the fast electron beam with increasing I_L. This is understood as follows: the magnetic field reversal driving the hollowing effect originates close to the edge of the beam (where target heating is of the order of a few eV), and therefore the radius of the ring is, to first order, defined by the overall beam divergence. The electron beam divergence, in turn, depends on the angular distribution of the electrons at the source (which is fixed in these simulations at 50° [8]) in conjunction with the strength of the collimating magnetic field. The field is strongest within the first few tens of microns from the front surface (where the current density is highest) − note that beam hollowing is not seeded until a depth of $\sim 40\mu m$ (as shown in figure 1(c)). In this region (i.e. closest to the front surface) the spatial profile of the electron beam can be approximated as a cylinder. The resistive azimuthal magnetic field encasing a uniform cylindrical electron beam of radius r_f can be estimated as $\partial \mathbf{B}/\partial t = \eta \mathbf{j}_f / r_f$, where the fast electron current is given by $\mathbf{j}_f = I_f/T_f$, in which I_f is the fast electron beam intensity. The inverse dependence of the strength of the collimating magnetic field on the fast electron energy T_f is due to the decrease in $\mathbf{j}_f$ as T_f is increased. T_f scales ponderomotively with the square root of the laser intensity, and hence as the peak laser intensity increases the magnetic field strength, and thus it's global pinching effect on the fast electron beam, decreases, increasing the overall beam divergence. Thus the radius of the ring induced by the hollowing component of the field formed near the edge of the beam increases with I_L.

For all three pulse parameter scans the ratio of the electron density in the annulus to the axial density is highest for $I_L = 5 \times 10^{20}$ Wcm^{-2} (as shown in figure 2(b)). Note that the same result at this intensity forms part of the simulation set for all three scans. For decreasing laser intensity, the overall beam divergence and ring radius decreases (due largely to the reduction in T_f, as discussed above) resulting in a higher beam density on-axis. Although hollowing still occurs at low I_L, the ratio of the beam densities in the annulus to the axial position decreases as the collimating magnetic field component dominates over the hollowing term (for small beam radii). As I_L becomes greater than 5×10^{20} Wcm^{-2}, the rate of the resistive magnetic field growth decreases. Thus, although the beam radius increases (which should act to enhance the ratio) the lower magnitude of the hollowing magnetic field, together with the higher T_f, results in less electrons being diverted into the annular structure. Since the local $\mathbf{j}_f$ of the annulus thereby decreases, the rate of localised resistive heating is lower and so the reinforcing feedback condition (as discussed previously) is not established − the ring structure does not develop properly in this case.

Conclusions

We have described how annular transport patterns of fast electron beams in silicon, driven by oppositely-directed azimuthal components of the self-generated resistive magnetic field, varies as a function of the parameters of the drive laser pulse. The results reveal an optimum peak laser intensity range for transporting fast electrons within a ring structure (produced in this way). The simulation results reveal that the size of the annulus increases with increasing peak laser intensity, driven by a decrease in the magnitude of the collimating magnetic field (which defines the overall beam divergence). Furthermore, we find an optimum laser intensity (i.e. $I_L = 5 \times 10^{20}$ Wcm^{-2}) for enhancing the annulus-to-axial electron density contrast ratio, determined by the relative strength of the resistive magnetic field components. Finally, we find that the size of the annular profile is particularly sensitive to the laser focal spot size, which enables some degree of control of the annular transport pattern given a fixed electron beam temperature or drive

laser intensity.

The study presented in this report is described in fuller detail in MacLellan *et al.* [10]. In addition, follow-up work on this scheme shows that the ring size can also be controlled by variation of lattice-melt gradients in the target [11].

References

[1] M. Tabak *et al.*, Phys. Plasmas 1, 1626 (1994).

[2] M. Borghesi *et al.*, Fusion Sci. Technol. 49, 412 (2006).

[3] P. McKenna *et al.*, Phys. Rev. Lett, 106, 185004 (2011).

[4] D. A. MacLellan *et al.*, Phys. Rev. Lett, 111, 167588 (2013).

[5] D. A. MacLellan *et al.*, Laser Part. Beams, 31, 475 (2013).

[6] S. Kar *et al.*, Phys. Rev. Lett. 102, 055001 (2009).

[7] S. C. Wilks and W. L. Kruer, IEEE J. Quantum Electron. 33, 1954 (1997).

[8] M. Coury *et al.*, Phys. Plasmas 20, 043104 (2013).

[9] M. P. Desjarlais, J. D. Kress, and L. A. Collins, Phys. Rev. E 66, 025401 (2002).

[10] D. A. MacLellan *et al.*, Plasma Phys. Control. Fusion., 56, 084002 (2014).

[11] D. A. MacLellan *et al.*, Phys. Rev. Lett, *At press* (2014).